Regular Article

ANALYTICAL AND BIOANALYTICAL CHEMISTRY RESEARCH

Published by the Iranian Chemical Society

Anal. Bioanal. Chem. Res., Vol. 7, No. 2, 263-280, June 2020.

Facile Synthesis of MIL-53(Fe) by Microwave Irradiation and its Application for Robust Removal of Heavy Metals from Aqueous Solution by Experimental Design Approach: Kinetic and Equilibrium

Maryam Ghanbarian[a,b], Sedigheh Zeinali[c,d,*], Ali Mostafavi[a] and Tayebe Shamspour[a]

[a]*Department of Chemistry, Faculty of Sciences, Shahid Bahonar University, Kerman, Iran*

[b]*Young Researchers Society, Shahid Bahonar University, Kerman, Iran*

[c]*Department of Nanochemical Engineering, School of Advanced Technologies, Shiraz University*

[d]*Nanotechnology Research Institute, Shiraz University*

(Received 18 February 2019 Accepted 23 June 2019)

MIL-53(Fe) with a huge porosity has been synthesized by microwave radiation in different conditions: various powers (80, 100 W) and time (5, 10 min). Nano-sized crystals were characterized using X-ray diffraction (XRD), scanning electron microscopy (SEM), Fourier transform infrared spectroscopy (FTIR), and specific surface area analysis. After characterization, MIL-53(Fe)-1 with the best porous structure for Pb(II) and Cd(II) removal was used for all tests from aqueous solution. The best condition for the synthesis was 5 min and 80 W. Then, the best porous structure was selected for removal of Pb(II)/Cd(II) from aqueous solution. The response surface methodology (RSM) based on central composite design (CCD) was applied to optimize the removal capacity. In these experimental designs, four independent variables were studied and the best condition was evaluated as pH (in the range of 6-8), temperature (40-50 °C), contact time (50 min), and adsorbent amount (0.1-0.3 g l^{-1}). The removal efficiency and capacity of MIL-53(Fe) for Pb(II) and Cd(II) were further surveyed. Langmuir equation was the best isotherm to describe the adsorption manner of Pb(II) and Cd(II) ions (q_{max} values (178.57 and 714.28 mg g^{-1}) for Pb(II) and Cd(II)). The adsorption process was confirmed by a pseudo-second-order kinetic pattern. The result of thermodynamic studies displayed that the sorption process was spontaneous and exothermal.

Keywords: MIL-53(Fe), Microwave radiation, Nano-sized crystals, Response surface methodology (RSM), Heavy metals, Removal

INTRODUCTION

With rapid development of the global economy, the heavy metals pollution has become critical and its effects on the environment and human health have attracted more and more attentions [1-3]. Heavy metals, such as cadmium and lead, are first pollutants in the waste water because of their easy solubility, high toxicity and bioaccumulation in the food chain.

Construction of new methods for the removal of heavy metals in the aqueous environment is important. So, many methods have been applied, such as chemical precipitation, reverse osmosis, conventional coagulation, ion exchange and adsorption. Among them, adsorption and ion exchange are simple and cost-effective method with respect to the other techniques [4-22].

Throughout the past decades, inorganic metal oxide materials have been applied as adsorbents for the removal of heavy metals, such as montmorillonite clay [23], kaolinite [24], zeolites [25,26] modified Fe_3O_4 particles [27] and activated carbon [28,29]. These adsorbents generally have low adsorption capacity for heavy metals because of the limited voids available among them.

Metal-organic frameworks (MOFs) are a fundamentally

*Corresponding author. E-mail: zeinali@shirazu.ac.ir

a new class of nanoporous materials [30,31]. The crystalline porous materials are built from transition metal ions and bridging organic ligands, which have an extensive, sturdy and open crystalline structure [32]. Owing to their extra-high porosity, ordered, and well characterized porous structures, adjustable chemical functionality and Host-guest interactions, MOFs porous materials are attracting increasing consideration due to the potential application in adsorption, separation, gas storage, and heterogeneous catalysis [33,34].

Whilst MOFs are conventionally produced by solvothermal reactions [35], alternative synthesis by microwave [36,37], sonochemical [38,39], electrochemical [40] and mechanochemical [41] methods have also been explored. Envisaged industrial applications of MOFs have motivated researchers to develop new methods for their synthesis. The new methods should provide benefits such as reduction in synthesis time, easy production scale-up, homogenous and high quality products. Among these, only microwave (MW) and sonochemical methods appear to be universally applicable for MOFs preparation as their reaction conditions can be easily adaptable from the conventional approaches [36-39,42-44].

MW irradiation is particularly promising technique due to the minimization of energy and optimization of reaction conditions. MW irradiation is characterized by accelerated reactions, as an effect of the intense localized heating, reaction times reduced from days and hours in classical heating to minutes and seconds. The magnitude of heating depends on the dielectric properties of the molecules, so produced energy is transmitted to the material directly and uniformly. This allows the all material to be heated quickly and simultaneously, resulting in homogeneous nucleation, fast crystallization, extensive reductions in particle size and higher efficiency [45,46].

One interesting aspect of certain MOF materials is an unusual solid-state flexibility. One famous flexible MOF is a material known as MIL-53 (Materials of Institut Lavoisier) [47]. This is a metal carboxylate with chemical formula 3D-[(M_4-bdc)(M-OH), where in 1,4-benzenedi-carboxylate is the organic linker and the metal is in the +3 oxidation state and can be Fe [48], Cr [47], Sc [49], Al [50] or Ga [51]. This material shows a significant 'breathing' feature. The breathing feature of the MIL-53 is related to the metal node. This material only enlarges in the proximity of guests [47-50].

So, this group of MOFs has many practical applications in removal of pollutants in large scale from liquid media.
In this work, we have developed rapid and energy efficient synthesis techniques utilizing MW irradiation to produce and analyze the crystallization of MIL-53(Fe), a flexible structure, environment friendly and non-toxic iron(III) benzenedicarboxylate MOF at a short time.

For the first time, we applied nanosize MIL-53(Fe) for removal of Pb(II) and Cd(II) from aqueous environments. These adsorbents had high adsorption capacity of heavy metals because of the huge voids available and their breathing feature. The focus of this research was to investigate a feasible method for MIL-53(Fe), synthesized as a nanosized sorbent, for removal of Pb(II) and Cd(II) from aqueous solutions as well as optimization of the process variables using the response surface modeling (RSM) approach. CCD was chosen to survey the individual and synergetic effects of factors such as contact time (min), temperature (°C), adsorbent dosage (g) and pH on the percentage removal of heavy metals as response.

MATERIALS AND METHODS

Apparatus

1,4-Benzenedicarboxylic acid H_2BDC (99%), $FeCl_3.6H_2O$, $Cd(NO_3)_2{\cdot}4H_2O$, $Pb(NO_3)_2$, N,N-dimethyl-formamide (DMF, 99%), were all of analytical grade and provided from Merck (Darmstadt, Germany). The stock solution of Pb(II) and Cd(II) was prepared by dissolving an adequate amounts of $Pb(NO_3)_2$ and $Cd(NO_3)_2.4H_2O$ in deionized water, respectively. The Pb(II) and Cd(II) solution was diluted with deionized water for various working concentrations for adsorption study.

Instrumentation

The developed adsorbent (MIL-53(Fe) nanosized) was characterized by X-ray diffractometer (XRD), Fourier transform infrared spectroscopy (FT-IR), scanning electron microscopy (SEM), and a specific surface area analyzer. The X-ray diffraction (XRD) patterns were registered by a PANalytical X'Pert PRO MPD instrument (PANalytical B.V., Almelo, The Netherlands) equipped with a back

monochromator acting at a tube voltage of 40 kV and a tube current of 30 mA using a copper cathode as the X-ray source (λ = 1.542 Å). The FTIR spectra (400-4000 cm^{-1}) of the adsorbent dispersed in KBr pellets were recorded by a Bruker tensor 27 spectrometer (Madison, WI, USA). SEM micrographs were obtained by a SEM, KYKY-EM model 3200 scanning electron microscopy (Zhongguancun Beijing, China) operating at 20 kV to investigate the morphology of the nanoporous structure of MIL-53(Fe). The BET surface areas and micropore size distributions of the materials were tested on a specific surface area analyzer (ASAP2020 Micromeritics setup), and the samples were degassed in a vacuum at 150 °C for about 3 h to remove water and other physically adsorbed species.

The pH evaluations were carried out using a digital pH meter Corning 125 equipped with a combined glass electrode. The pH value was fixed by the addition of 1 M HCl or NaOH solution. The concentration of ions was determined by a Varian model Spectra AA 220 (Murglave, Australia) atomic absorption spectrometer.

Synthesis of MIL-53(Fe) by MW Irradiation

The MIL-53(Fe) samples were synthesized by dissolving 1.621 g of $FeCl_3.6H_2O$ and 0.996 g of H_2BDC in 30 ml of DMF, separately. The solution was subjected to a predetermined power (*i.e.* 80 or 100 W) and time (*i.e.* 5 or 10 min). After completion of each reaction and prior to characterization, products were cooled at room temperature and centrifuged, then several times washed with DMF and dried overnight (Table 1).

General Procedure for Removal of Pb(II) and Cd(II) Ions

In order to study the adsorption capacity of MIL-53(Fe)-1 for Pb(II) and Cd(II) ions, the effect of several factors, pH value (2-10), contact time (10-120 min), sorbent dosage (0.1-1.0 g l^{-1}) and reaction temperature (25-65 °C) on the adsorption experiments were investigated. In a glass flask, dried MIL-53(Fe) material was mixed with certained Pb(II)/Cd(II) solution and the mixture was stirred before centrifugation. The concentrations of remained Pb(II)/Cd(II) ions in the supernatants were then measured by atomic absorption spectroscopy (AAS) and the sample absorbance was measured. The removal percentages of ions were calculated using the following equation:

$$\%\,\mathrm{Re}moval = \frac{C_0 - C_e}{C_0} \times 100$$

where C_o and C_e are the initial and final concentrations (mg l^{-1}) of Pb(II)/Cd(II) in solution, respectively.

Optimization

A full factorial design consisting of 30 experimental runs with 6 runs at the center point was used for screening and modeling of the effective parameters on the Pb(II)/Cd(II) removal from the solution, separately. Four variables in the experiment process *via* sample contact time (A; 10-120 min), temperature (B; 25-65 °C), pH (C; 2-10) and adsorbent dose (D; 0.1-1.0 g l^{-1}) were selected to be analyzed, aiming to figure out their influence on the removal process. Then, the analysis of variance (ANOVA) was carried to accredit the model. However, the related models are pretty confined to only two levels in these types of designs. So, a second-order model (response surface design) which provides more than two levels for fitting of a full quadratic model [52] is necessary to find the best conditions for removal study. Finally, an experiment was again carried under optimal conditions to validate the defined model. The Design Expert Version 7.0 software was used to develop the experimental plan for RSM.

RESULTS AND DISCUSSION

Characterization of the Synthesized Adsorbent

X-Ray diffraction (XRD). The XRD pattern of samples are plotted in Figs. 1a-d. As can be seen in Fig. 1, only the pattern of MIL-53(Fe)-1 shows a flat background and high intensities, indicating high crystallinity of this sample. Additionally, no other phases were detected, indicating high purity of the sample. In the pattern of the sample, the main diffraction peaks appearing at 2θ of 9.24, 12.7, 18.24, 18.58, 22.1, 25.52, 27.32, 29.8, 30.28, 36.18 are identical to those reported for the MIL-53(Fe) phase [47,53-54].

Fourier transform infrared spectroscopy (FTIR). In order to analyze the molecular structure and recognize the functional groups of MIL-53(Fe) samples, the FTIR spectroscopy was performed and the result is shown in Figs.

Table 1. Synthesis Condition for MIL-53(Fe) Synthesized by MW Irradiation

Sample code	MW time (min)	MW power (W)
MIL-53(Fe)-1	5	80
MIL-53(Fe)-2	5	100
MIL-53(Fe)-3	10	80
MIL-53(Fe)-4	10	100

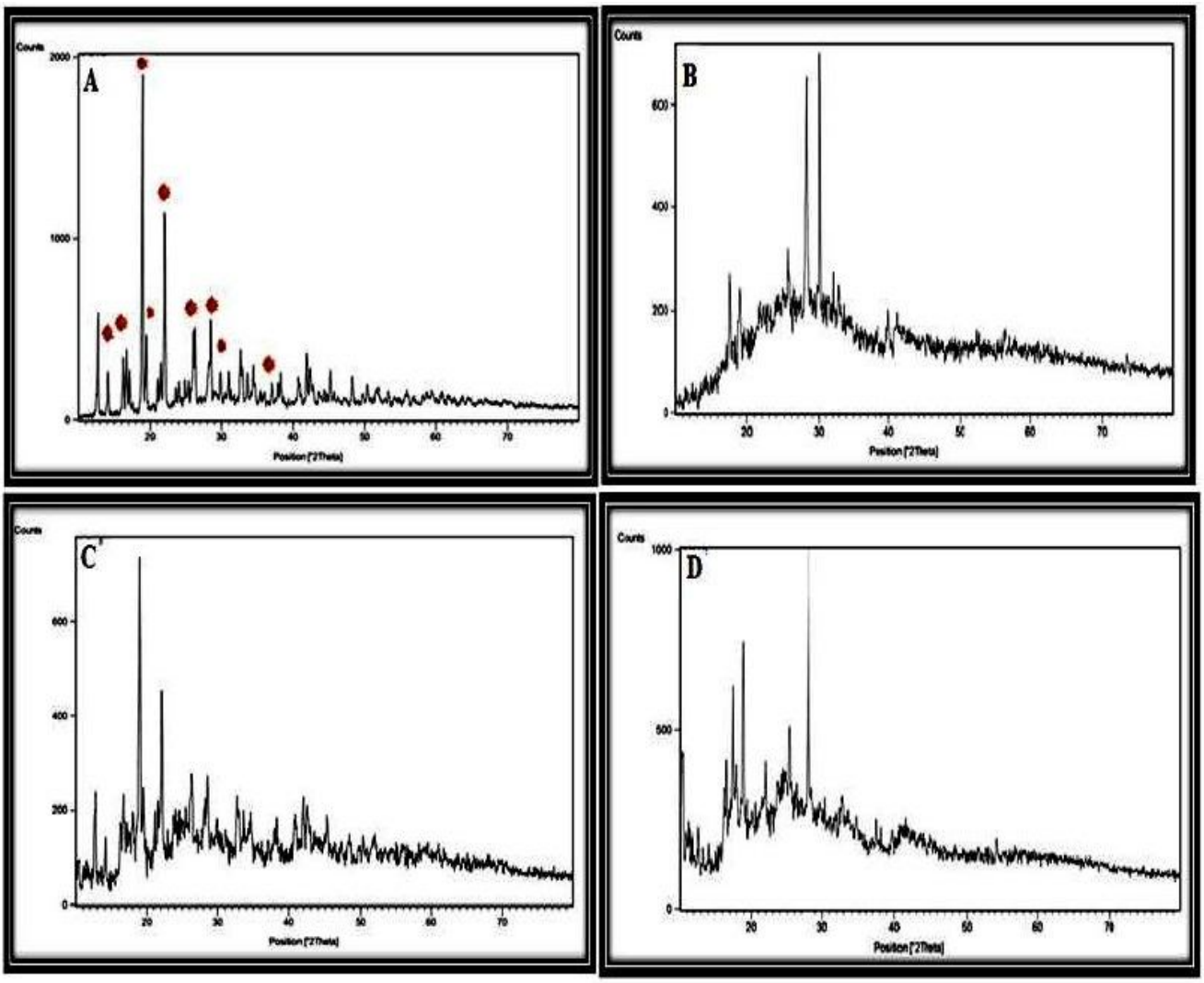

Fig. 1. XRD patterns of sample 1 (a), sample 2 (b), sample 3 (c), and sample 4 (d).

Table 2. Textural Properties of Sample

Sample	S_{BET} ($m^2\ g^{-1}$)	$S_{Langmuir}$ ($m^2\ g^{-1}$)	Pore volume ($cm^3\ g^{-1}$)	Pore size (Å)
MIL-53(Fe)	71.9321	96.1814	0.04294	684.462

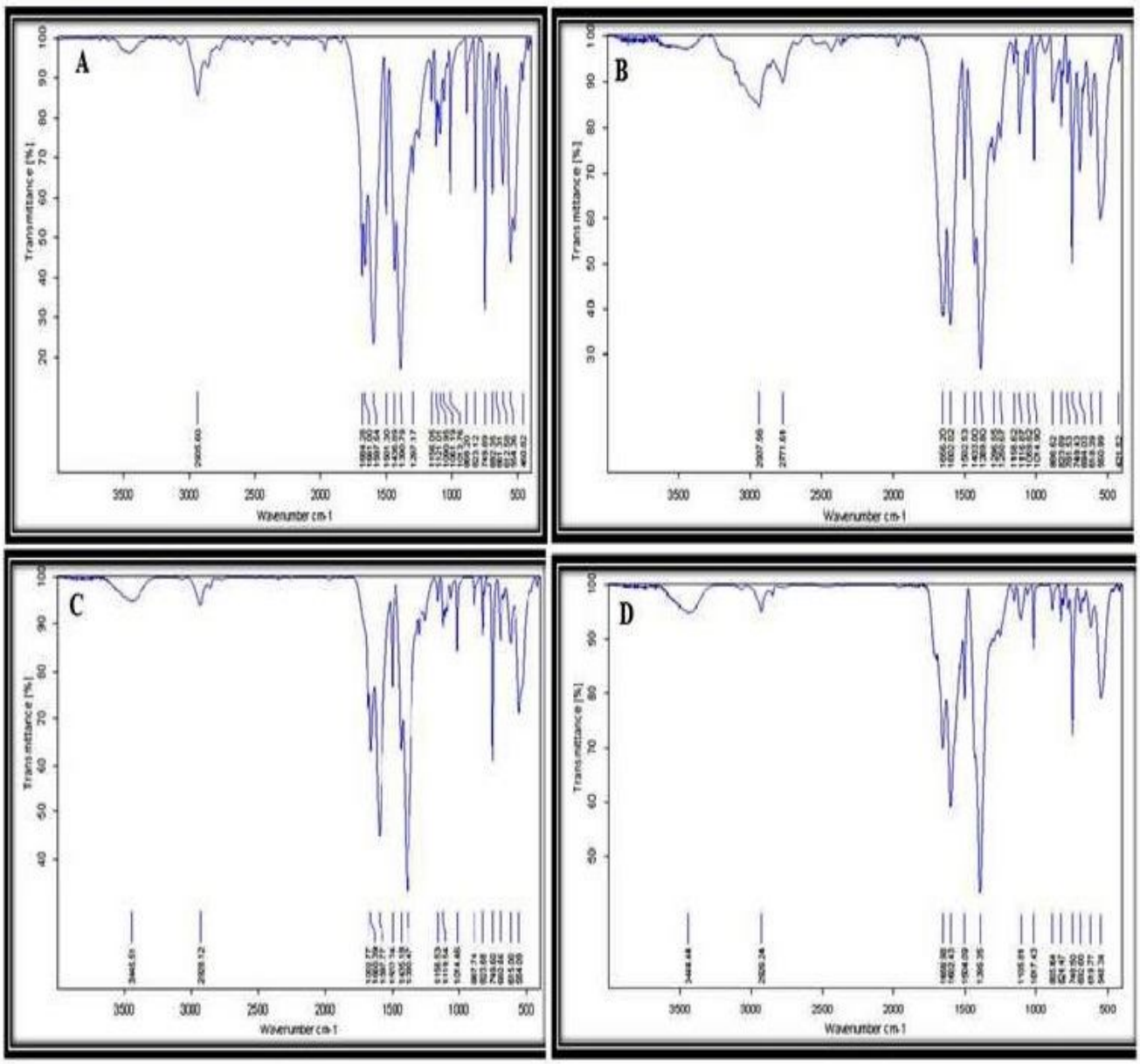

Fig. 2. FT-IR spectra of sample 1 (a), sample 2 (b), sample 3 (c) and sample 4 (d).

2a-d. As a comparison, in the spectrum of samples, we measured the ratio of intensities of the characteristic band of the MIL-53(Fe) framework located at ~823 cm^{-1}. As can be seen in Fig. 2, MIL-53(Fe)-1 shows the highest intensities at ~823.1 cm^{-1}. The other characteristic absorption peaks of the MIL-53(Fe) sample appeared at 1669.2, 1597.5, 1501.3, 1390.8, 1013.7 cm^{-1}, which mainly resulted from the carboxylate groups vibrations, similar to those of reported data in the literature [55-58]. The slightly broadened band at 3442 cm^{-1} was related to stretching vibrations of hydroxyl groups from iron oxide. The two sharp peaks at 1501.3 and 1390.8 cm^{-1} are assigned to asymmetric (ν_{as} (C-O)) and symmetric (ν_{s} (C-O)) vibrations of carboxyl groups, respectively, confirming the presence of a dicarboxylate linker within the sample. The peak at 749.9 cm^{-1} corresponds to the C-H bending vibrations of benzene and the intense peak at 554 cm^{-1} is related to Fe-O vibrations [59].

Scanning electron microscopy (SEM). The MIL-53(Fe) crystals synthesized under MW conditions produced small and homogeneous crystals, a clear indication of the efficiency of this synthesis method. As can be seen in Fig. 3, among four samples, the particles of MIL-53(Fe)-1 showed approximate size of 50-80 nm and hexagonal bipyramidal morphologies (Figs. 3a and b). Reduction of size is generally due to synthesis of the crystals under MW conditions -a phenomenon which can be attributed to the uniform and fast nucleation.

N_2 adsorption-desorption isotherms. The porosities of MIL-53(Fe)-1 sample were evaluated by nitrogen adsorption analysis. The porosity and surface area of the sample is presented in Table 2. According to BET theory, the specific surface area was calculated as 71.93 m^2 g^{-1} for MIL-53(Fe).

This surface area observed for MIL-53(Fe) indicates that the anhydrous form of MIL-53(Fe) exhibits closed pores with approximately no available porosity to nitrogen gas. As mentioned elsewhere [60,61], pores of MIL-53(Fe) are only opened in the presence of guest molecules, however, the synthesize MIL-53(Fe) in this research has a higher surface area than other MIL-53(Fe) samples reported previously [60,61].

Screening of the Effective Parameters Using Central Composite Design

A statistic design of experiment is prior in order to reduce the number of experiments and consider all probable interactions between the variables [52]. Experimental design sequence was randomized in order to avoid the effects of uncontrolled factors. By ANOVA analysis, some effective parameters, such as critical factor effects, interactions and model efficiency were investigated. Tables 3 and 4 reveals that the criterion for significant contribution of each variable is P value (less than 0.05) and F value (more than 0.05) by considering 95% confidence level. The basic interactions and quadratic effects were considered in this design. The data analysis by response surface methodology (RSM) for plotting recovery (R%) *vs.* main variables was investigated and the results are depicted in Fig. 4. The pH value plays a unique role on interaction between sites of sorbent-ions and subsequent removal of ions. As indicated in Figs. 4a, b-d, e, at the pH-values higher than 7, metal ions could precipitate as hydroxyl complexes at the presence of alkaline ions. At lower pH values, the hydrogen ions compete with the Pb(II)/Cd(II) ions for the available sorption sites, thus the removal efficiency decreases. Therefore, the suitable pH value for Pb(II)/Cd(II) removal was between 6 and 8. During the removal process, the least amount of sorbent was needed to obtain satisfactory recovery. The best removal efficiency for Pb(II) and Cd(II) ions were 0.1 g l^{-1} and 0.3-0.55 g l^{-1}, respectively. So, according to Figs. 4b-e, the suitable sorbent dosage for Pb(II) and Cd(II) removal was between 0.1 and 0.3 g l^{-1}.

The effects of contact time in the range of 10-120 min (Figs. 4c, f) reveal that the best recovery was obtained after 50 min. Effect of temperature on the adsorption capacity of MIL-53(Fe) for Pb(II) and Cd(II) were investigated in the temperature range of 25-65 °C. As shown in Figs. 4a, c-d, f, when the adsorption occurred in the temperature range from 25-40 °C, the removal efficiency of Pb(II) and Cd(II) increased with the increase of temperature. However, the removal efficiency of Pb(II) and Cd(II) was constant in the temperature range of 40-50 °C. This might be due to increase in the mobility of Pb(II)/Cd(II) ions with a rise in

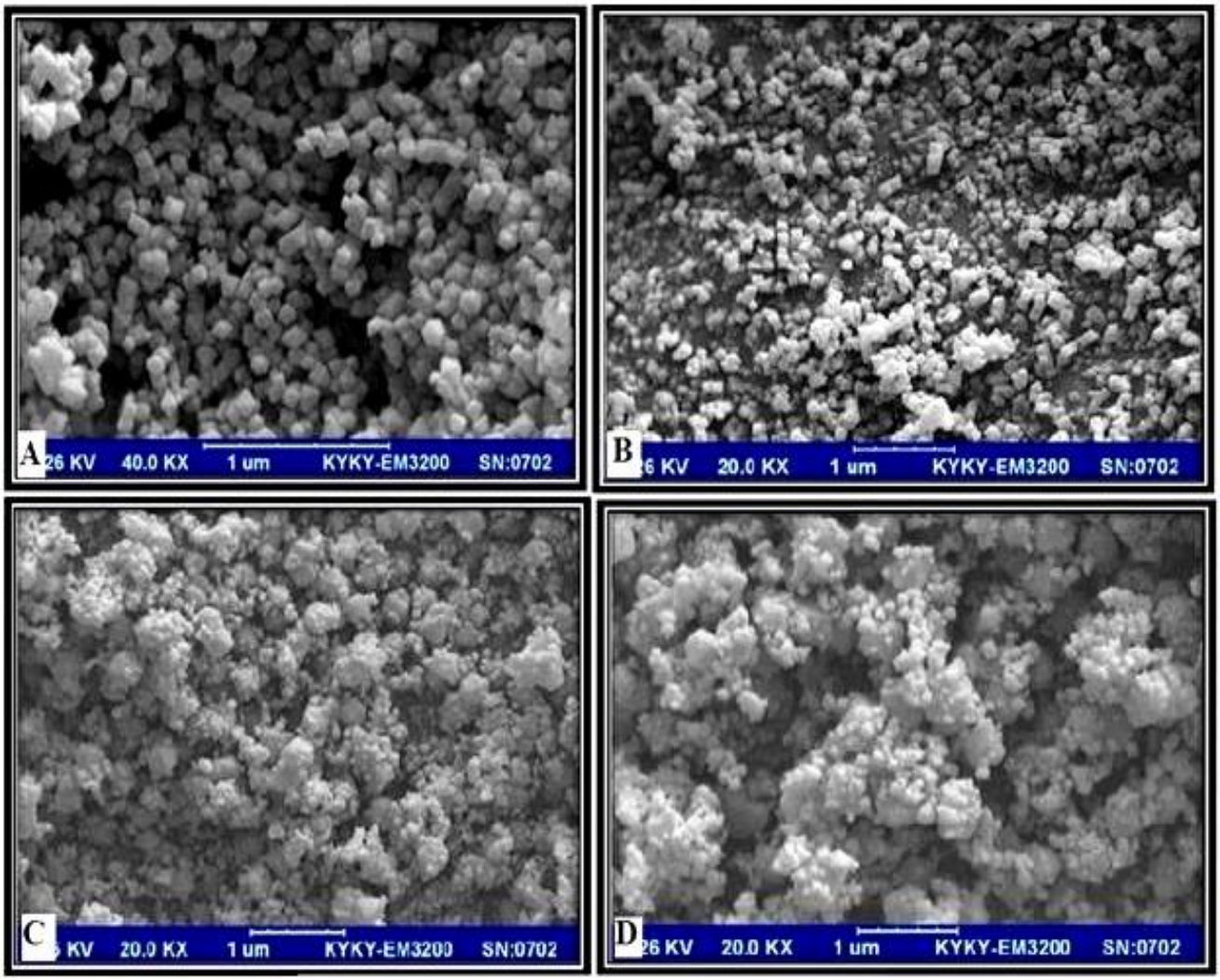

Fig. 3. Typical SEM images of fully crystallized sample 1 (a: 40 KX, b: 20 KX), sample 2 (c), sample 3 (d) and sample 4 (e).

temperature.

Kinetics models. To investigate the controlling mechanism of the adsorption processes such as mass transfer and rate controlling step in the removal of Pb(II) and Cd(II) ions from solution by nanosize MIL-53(Fe), the kinetic modeling of the process using pseudo-first-order (Eq. (2)) and pseudo-second-order (Eq. (3)) are applied to model the kinetics

$$\ln(q_e - q_t) = \ln q_e - k_1 t \quad (2)$$

$$\frac{t}{q_t} = \frac{1}{k_2 q_e^2} + \frac{t}{q_e} \quad (3)$$

where q_e and q_t are the amounts of adsorbate (mmol g^{-1}) at equilibrium and at any given time t (min), respectively. Also, k_1 (min^{-1}) and k_2 (g $mmol^{-1}$ min^{-1}) are the rate constants for the pseudo-first-order and the pseudo-second-order models, respectively.

In this kinetics models, plots of $\ln(q_e - q_t)$ *vs.* t and t/q_t *vs.* t give straight lines (see Figs. 5a, b) for calculating q_e, k_1 and k_2. The obtained results are summarized in

Table 3. ANOVA Results for the Response Surface Quadratic Model for Cd(II) Removal

Source	Sum of squares	DF	Mean squares	F-value	p-value Prob > F	Remarks
Model	848.48	14	60.61	41.72	<0.0001	Significant
A-contact time	0.042	1	0.042	0.029	0.8678	
B-temperature	77.04	1	77.04	53.03	<0.0001	Significant
C-pH	48.74	1	48.74	33.55	<0.0001	Significant
D-sorbent dosage	292.60	1	292.60	201.41	<0.0001	Significant
AB	63.20	1	63.20	43.50	<0.0001	Significant
AC	52.56	1	52.56	36.18	<0.0001	Significant
AD	1.56	1	1.56	1.08	0.3161	
BC	18.06	1	18.06	12.43	0.0031	Significant
BD	3.06	1	3.06	2.11	0.1671	
CD	0.30	1	0.30	0.21	0.6547	
A^2	32.07	1	32.07	22.07	0.0003	Significant
B^2	149.07	1	149.07	102.61	<0.0001	Significant
C^2	25.08	1	25.08	17.26	0.0008	Significant
D^2	65.37	1	65.37	44.99	<0.0001	Significant
Residual	21.79	15	1.45			
Lack of fit	15.34	10	1.53	1.19	0.4495	Not Significant
Pure error	6.45	5	1.29			
Cor. Total	870.27	29				

Table 7 confirming that the pseudo-second order kinetics model can better fit to the model for describing the process. This model indicates that the overall process dependents on the amount of Pb(II) and Cd(II) in the solution and on the availability of adsorption sites on the adsorbents [63,64].

Adsorption Isotherms

Interaction between adsorbent and adsorbate is described with adsorption isotherms. The adsorption isotherm indicates how the adsorbed molecules distribute between the liquid phase and the solid phase when the adsorption process reaches an equilibrium state. The analysis of the isotherm data by fitting them to different isotherm models is an important step in finding a suitable model that can be used for design purpose. Several models of adsorption have been used to illustrate adsorption equilibrium. In this study, Langmuir and Freundlich models are applied to describe the adsorption isotherms. The

Table 4. ANOVA Results for the Response Surface Quadratic Model for Pb(II) Removal

Source	Sum of squares	DF	Mean squares	F-value	p-value Prob > F	Remarks
Model	1067.45	14	79.25	59.75	<0.0001	Significant
A-contact time	31.51	1	31.51	24.69	0.0002	
B-temperature	46.20	1	46.20	36.21	<0.0001	
C-pH	263.34	1	263.34	206.37	<0.0001	
D-sorbent dosage	143.57	1	143.57	112.51	<0.0001	
AB	56.63	1	56.63	44.38	<0.0001	
AC	48.65	1	48.65	38.13	<0.0001	
AD	29.98	1	29.98	23.49	0.0002	
BC	3.90	1	3.90	3.06	0.1008	
BD	6.13	1	6.13	4.80	0.0447	
CD	36.30	1	36.30	28.45	<0.0001	
A^2	160.05	1	160.05	125.43	<0.0001	
B^2	253.59	1	253.59	198.73	<0.0001	
C^2	65.10	1	65.10	51.02	<0.0001	
D^2	65.10	1	65.10	51.02	<0.0001	
Residual	83.47	15	1.28			
Lack of fit	80.91	10	1.63	2.88	0.1275	Not significant
Pure error	2.83	5	0.57			
Cor. Total	1110.08	29				

linearized Langmuir and Freundlich isotherms are explained by the following equations [65-67]:

Langmuir model:

$$\frac{C_e}{q_e} = \frac{1}{k_L q_{\max}} + \frac{C_e}{q_{\max}} \quad (4)$$

Freundlich model:

$$\log q_e = \log k_F + \left(\frac{1}{n}\right)\log C_e \quad (5)$$

where C_e (mg l^{-1}) and q_e (mg g^{-1}) are, respectively, the concentration and adsorbed amount of Pb(II)/Cd(II) at adsorption equilibrium, k_l is the Langmuir constant (l g^{-1}), k_f is the Freundlich constant ($mg^{1-(1/n)}/l^{1/n}/g$), and q_m is the maximum adsorption capacity (mg g^{-1}).

The Langmuir and Freundlich constants are summarized in Table 6. By comparing the adsorption equilibrium of Pb(II)/Cd(II) with the Langmuir and Freundlich models, it is found that the experimental results are in conformity with Langmuir isotherm rather than with the Freundlich model.

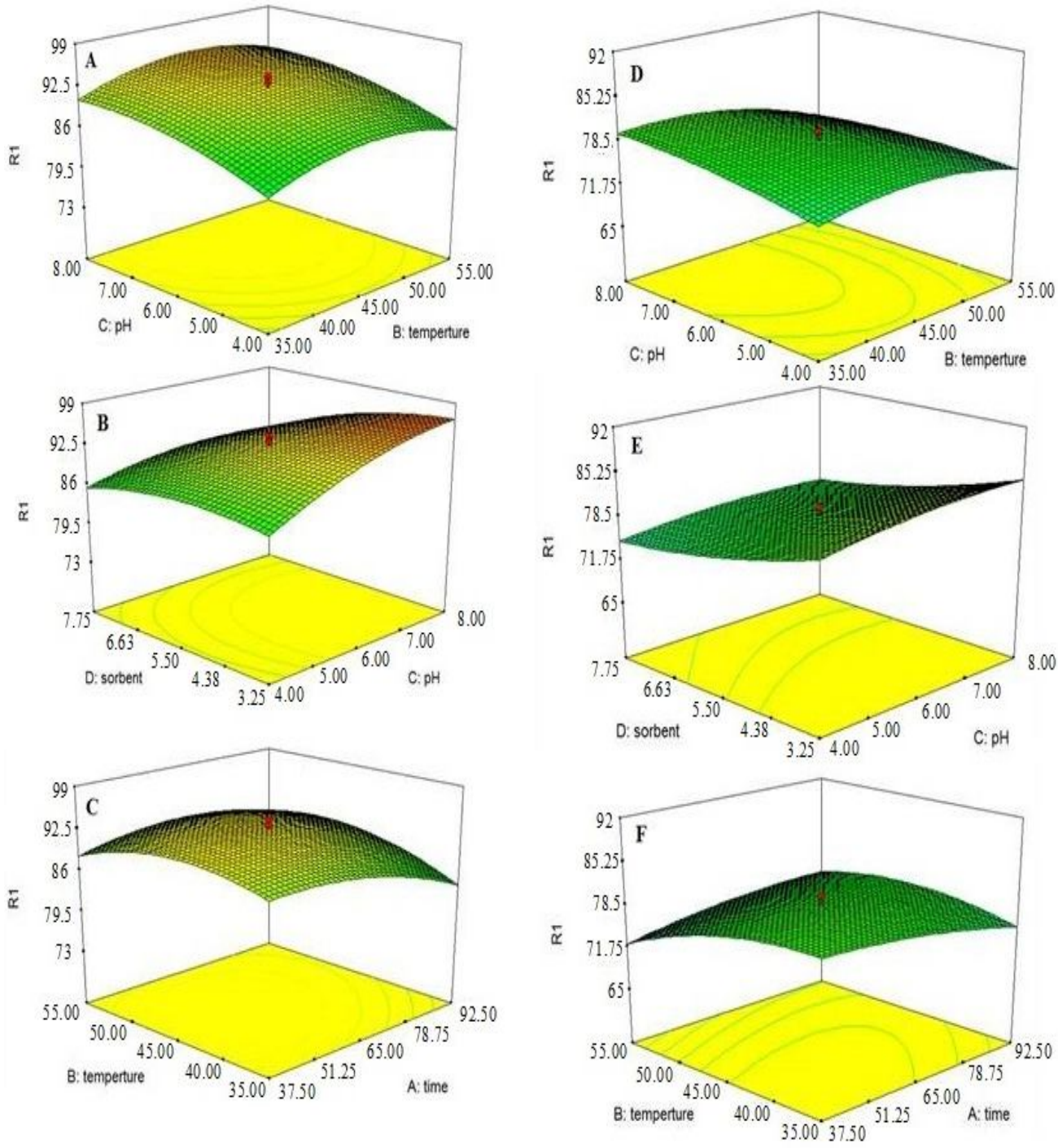

Fig. 4. Response surface plots and interactions of pH and temperature (a), pH and adsorbent dosage (b), time and temperature (c), pH and temperature (d), pH and adsorbent dosage (e), and time and temperature (f) for Pb(II) and Cd(II) removal by MIL-53(Fe).

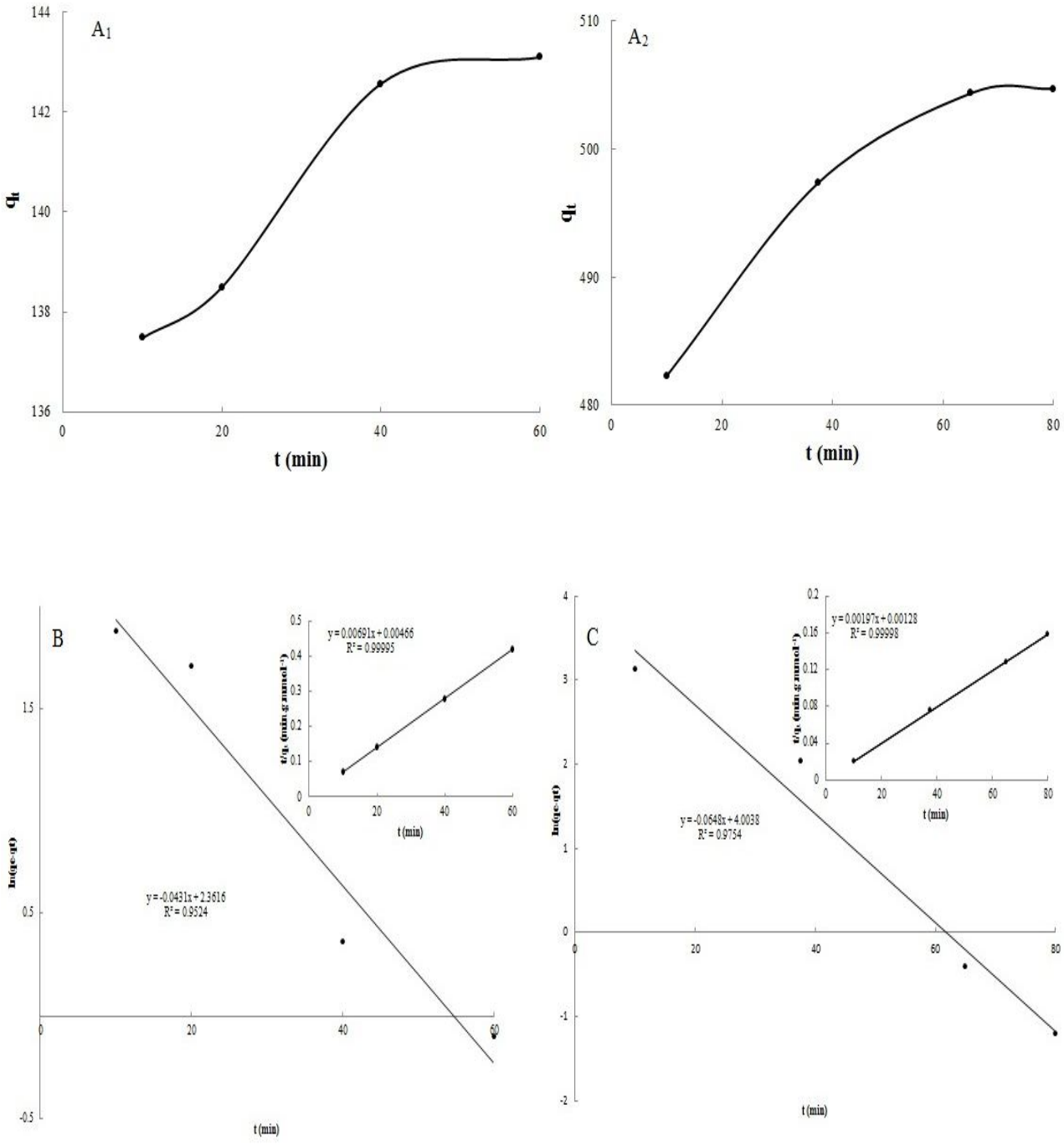

Fig. 5. a. Effect of equilibrium time on adsorption of MIL-53(Fe) for, (A_1): Pb(II) and (A_2): Cd(II) removal. b. Linearized first-order rate equation plots for Pb(II) removal by MIL-53(Fe), Inset: linearized second-order rate equation plots for Pb(II) removal by MIL-53(Fe). c. Linearized first-order rate equation plots for Cd(II) removal by MIL-53(Fe), Inset: linearized second-order rate equation plots for Cd(II) removal by MIL-53(Fe).

Table 5. The ANOVA Results of Second-order Regression Model for Cd(II) Removal

Std. Dev.	1.21	R-Squared	0.9750
Mean	66.72	Adj R-Squared	0.9516
C.V.%	1.81	Pred R-Squared	0.8878
PRESS	97.66	Adeq Precision	30.604

Table 6. The ANOVA Results of Second-order Regression Model for Pb(II) Removal

Std. Dev.	1.13	R-Squared	0.9824
Mean	76.00	Adj R-Squared	0.9659
C.V.%	1.49	Pred R-Squared	0.9098
PRESS	98.01	Adeq Precision	30.396

Table 7. The Constants and Correlation Coefficients of Pseudo-first Order and Pseudo-second Order Kinetic Models for Adsorption of Cd^{2+}/Pb^{2+} onto MIL-53(Fe)

	C_0 (mg l^{-1})	q_e (exp)[a] (mg g^{-1})	Pseudo-first-order model			Pseudo-second-order model		
			q_e[a] (mg g^{-1})	k_1 (min^{-1})	R^2	q_e[a] (mg g^{-1})	k_2 (g mg^{-1} min^{-1})	R^2
Pb(II)	30	143	10.60	0.0431	0.9524	144.7	1.50	0.9999
Cd(II)	30	504	54.80	0.0648	0.9754	507.61	1.55	0.9999

[a]q_e (exp) and q_e are the experimental and calculated values of q_e, respectively.

Table 8. Langmuir, Freundlich and Temkin Adsorption Isotherm Constants for Cd^{2+}/Pb^{2+} Adsorption on MIL-53(Fe)

		Langmuir model			Freundlich model		
	q_e (experimental) (mg g^{-1})	q_{max} (mg g^{-1})	K_l (l g^{-1})	R^2	n	K_f (mg g^{-1})	R^2
Pb(II)	177	178.57	0.10	0.9972	2.46	26.96	0.976
Cd(II)	711	714.28	0.93	0.9991	3.04	276.44	0.9459

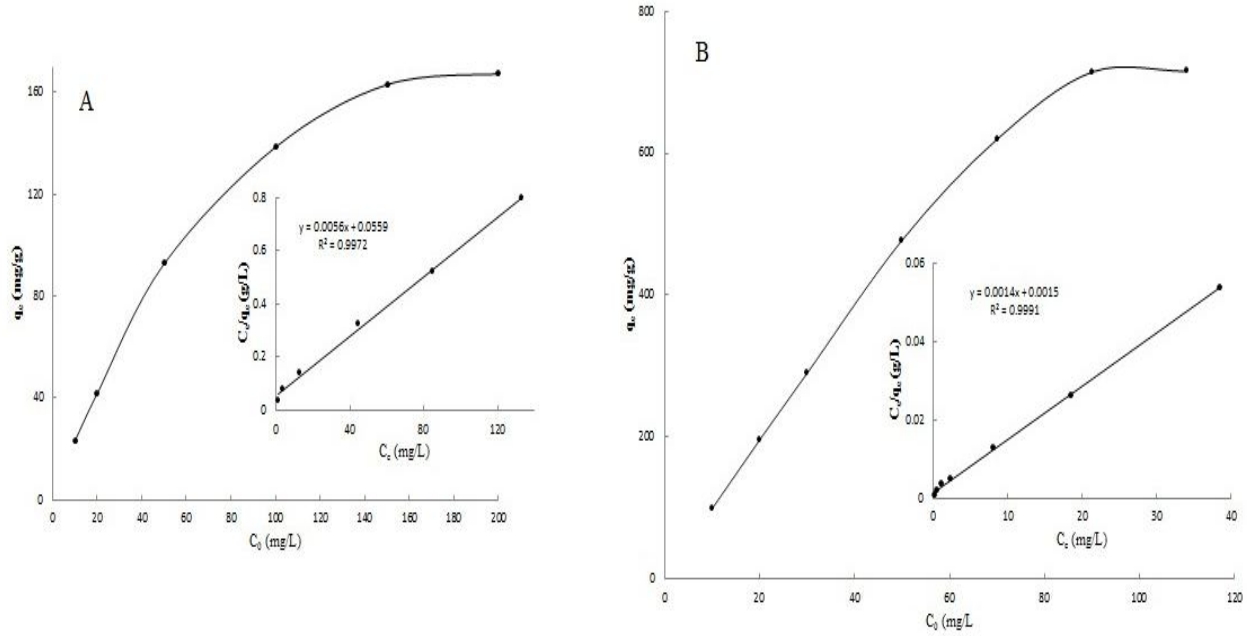

Fig. 6. (a) Adsorption capacities of MIL-53(Fe) for Pb(II), Inset: fitted Langmuir equation of MIL-53(Fe) and (b) Adsorption capacities of MIL-53(Fe) for Cd(II), Inset: fitted Langmuir equation of MIL-53(Fe).

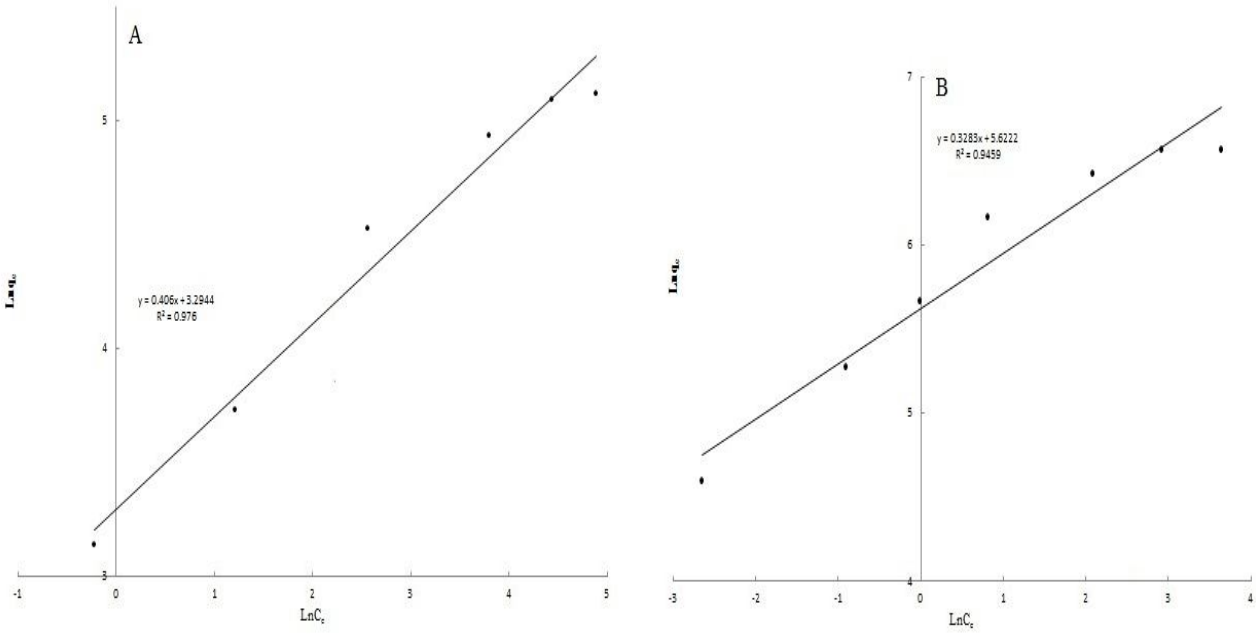

Fig. 7. (a) Freundlich equation of MIL-53(Fe) for Pb(II) and (a) Freundlich equation of MIL-53(Fe) for Cd(II).

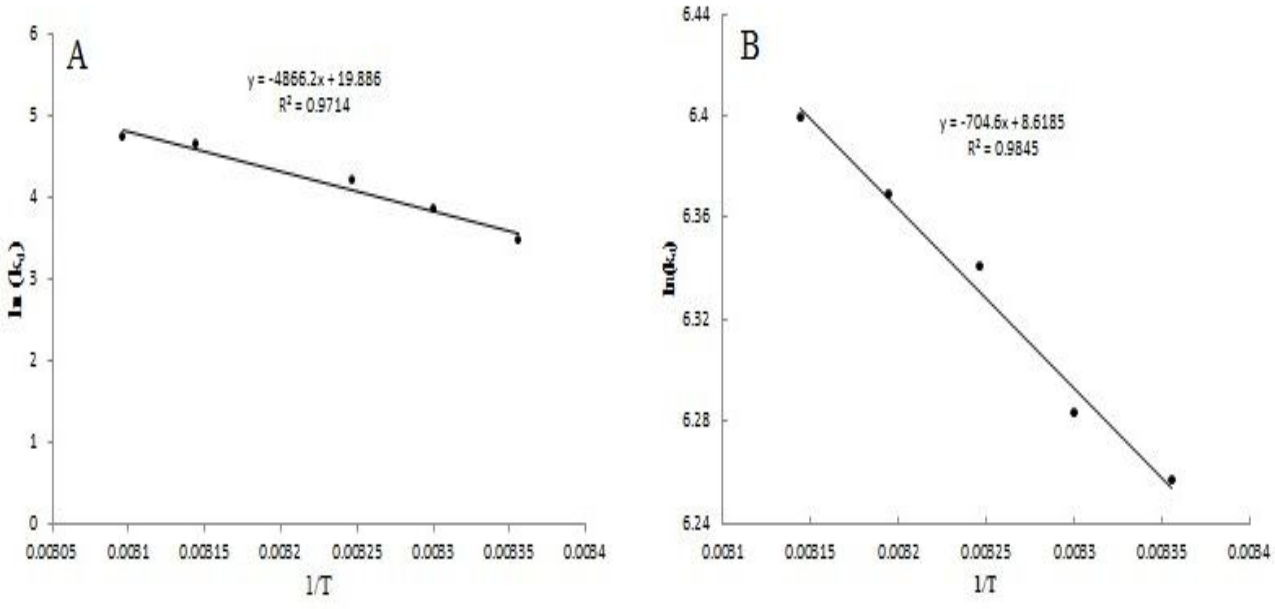

Fig. 8. Van't Hoff plots for the uptake of a) Pb(II). b) Cd(II) on the MIL-53(Fe).

Table 9. Thermodynamic Parameters at Different Temperatures

	ΔH	ΔS	ΔG		
	(J mol^{-1})	(J mol^{-1} K^{-1})	(kJ mol^{-1})		
			297	303	323
Pb(II)	-4457	165.33	-53.560	-54.551	-57.858
Cd(II)	-5858	71.65	-27.138	-27.567	-29.000

According to the slope and intercept in Figs. 6, 7a, b, the values of experimental q_{max} (177 and 711 mg g^{-1}) are very close to the respective calculated q_{max} values (178.57 and 714.28 mg g^{-1}) for Pb(II) and Cd(II), indicating that the sorption sites are basically homogeneous.

Thermodynamic Studies

Thermodynamic parameters such as the standard Gibbs free energy of the adsorption ΔG°, standard entropy of adsorption (ΔS°) and standard enthalpy of adsorption (ΔH°) provide additional information on inherent energetic changes of adsorption process, which can be calculated by using Eqs. (6) and (7):

$$\Delta G^{\circ} = -RT \ln K_d \quad (6)$$

$$\ln K_d = \frac{\Delta S^{\circ}}{R} - \frac{\Delta H^{\circ}}{RT} \quad (7)$$

where k_d is the distribution coefficient ($k_d = q_e/C_e$), T is the temperature, and R is the gas constant (8.314 J mol^{-1} K^{-1}). The values of (ΔH°) and (ΔS°) were evaluated from the slope and intercept of the Van't Hoff linear plot of ln(k_d) against 1/T (Figs. 8a, b). It can be seen in Table 9 that all

Table 10. Comparison of Maximum Adsorption Capacity of Metal Ions on Various Adsorbents

	Adsorbent	q_0 (mg g^{-1})	Ref.
Cd^{2+}	MIL-53(Fe)	714.28	This work
	Peels of banana	5.71	[69]
	$[CH_3NH_3]_{2X}Mn_x$-S_6.0.5H_2O	1.11	[70]
	Thiosemicarbazide modified chitosan	257.2	[71]
	Fe_3O_4-SO_3HMNP	80.9	[72]
Pb^{2+}	MIL-53(Fe)	178.57	This work
	Peels of banana	2.18	[69]
	Fe_3O_4@SiO_2-IIP	32.58	[73]
	$[CH_3NH_3]_{2X}Mn_x$-S_6.0.5H_2O	5.0	[70]
	Fe_3O_4-SO_3HMNP	108.93	[72]

values obtained for ΔG° are negative, suggesting the spontaneous nature of the Pb(II)/Cd(II) adsorption by MIL-53(Fe). The observed reduction in negative values of ΔG^0 with increasing temperature shows that the adsorption became less favorable at higher temperatures. It has been reported that ΔGº values between -20 and 0 kJ mol^{-1} are consistent with electrostatic interaction between sorption sites and the metal ion (physical adsorption), while ΔGº values in a range of -80 to -400 kJ mol^{-1} involve charge sharing or transfer from the biomass surface to the metal ion to form a coordinate bond (chemical adsorption) [68]. The amounts of ΔG° obtained in this research are within the ranges of -20 and 0 kJ mol^{-1}, indicating that physisorption is the dominate mechanism. On the other hand, the observed negative value of ΔH° (Table 9) indicates that the process is exothermic, while the positive value of ΔS° corresponded to an increase in randomness at the solid/solution interface during the adsorption of Pb(II)/Cd(II) by MIL-53(Fe).

Comparing our Research Results with Related Reports

Table 10 compares the adsorption capacity of Pb(II) and Cd(II) on various adsorbents. As show by the data, MIL-53(Fe) nano porous has the highest adsorption capacity compared to the other adsorbents. So, it is evident that MIL-53(Fe) nano porous shows a great potential as an adsorbent for Pb(II) and Cd(II) meatal ions [69-73].

CONCLUSIONS

In this work, MIL-53(Fe), a kind of metal-organic framework (MOF) material, has been synthesized by microwave (MW) irradiation. Small and homogeneous crystals were synthesized as quickly as 5 min from MW irradiation. The size reduction of crystals synthesized under this condition may be attributed to fast and uniform nucleation. To the best of our knowledge, these are the quickest crystallization times reported for MIL-53(Fe).

MIL-53(Fe) was proved to be an effective adsorbent for Pb(II) and Cd(II) removal from water. In the hydrated form, the pores of MIL-53(Fe) are filled with water molecules. Thus, MIL-53(Fe) showed a very high adsorption capacity of Pb(II)/Cd(II) in aqueous solution. To the best of our knowledge, this is the first work reporting the very high Pb(II) and Cd(II) adsorption capacity of MIL-53(Fe) with a Q_{max} of 178.57 and 714.28 mg g^{-1}, respectively.

A CCD was applied to determine the factors interaction and the optimum values of four significant parameters. A quadratic model was obtained from this design using Design Expert software. Central composite design (CCD) and laboratory experiments were significant to evaluate the adsorption process.

The adsorption experiments showed that MIL-53(Fe) had an excellent adsorption performance for heavy metal ions such as high adsorption ability and fast adsorption rate. The temperature variation has been used to evaluate the values of G°, H° and S°. So, values of G° and H° show the spontaneous and exothermic nature of the sorption process. The understudy equilibrium is best described by Langmuir sorption. The comparison of two kinetic models demonstrates that the adsorption kinetic can be well described by the second-order rate equation isotherm.

REFERENCES

[1] M. Kilic, C. Kirbiyik, O. Cepeliogullar, A.E. Putun, Appl. Surf. Sci. 283 (2013) 856.

[2] H. Wang, X. Yuan, Y. Wu, H. Huang, G. Zeng, Y. Liu, X. Wang, N. Lin, Y. Qi, Appl. Surf. Sci. 279 (2013) 432.

[3] Y. Liu, X. Sun, B. Li, Carbohyd. Polym. 81 (2010) 335.

[4] M. Naushad, Chem. Eng. J. 235 (2014) 100.

[5] S.A. Kim, S. Kamala-Kannan, K.J. Lee, Y.J. Park, P.J. Shea, W.H. Lee, H.M. Kim, B.T. Oh, Chem. Eng. J. 217 (2013) 54.

[6] H. Dogan, Toxicol. Environ. Chem. 94 (2012) 482.

[7] V. Gupta, M. Gupta, S. Sharma, Water Res. 35 (2001) 1125.

[8] M.T. Alvarez, C. Crespo, B. Mattiasson, Chemosphere 66 (2007) 1677.

[9] S. Bhattacharjee, S. Chakrabarty, S. Maity, S. Kar, P. Thakur, G. Bhattacharyya, Water Res. 37 (2003) 3954.

[10] Y. Hashimoto, T. Sato, Chemosphere 69 (2007) 1775.

[11] I.S. Ismael, A. Melegy, T. Kratochvil, Geotech. Geol. Eng. 30 (2012) 253.

[12] M. Kragovic, A. Dakovic, Z. Sekulic, M. Trgo, M. Ugrina, J. Peric, G. Diego, Appl. Surf. Sci. 283 (2013) 764.

[13] T. Madrakian, A. Afkhami, M. Ahmadi, Chemosphere 90 (2013) 542.

[14] R. Naseems, S.S. Tahir, Water Res. 35 (2001) 3982.

[15] Q. He, D. Yang, X. Deng, Q. Wuc, R. Li, Y. Zhai, L. Zhang, Water Res. 47 (2013) 3976.

[16] D.S. Dlamini, A.K. Mishra, B.B. Mamba, J. Appl. Pol. Sci. 22 (2011) 342.

[17] S.H. Abdel-Halim, A.M.A. Shehata, M.F. El-Shahat, Water Res. 37 (2003) 1678.

[18] K.K. Wong, C.K. Lee, K.S. Low, M.J. Haron, Chemosphere 50 (2003) 23.

[19] H.A. Kim, K.Y. Lee, B.T. Lee, S.O. Kim, K.W. Kim, Water Res. 46 (2012) 5591.

[20] E. Saifullah, M. Meers, P. Qadir, F.M.G. de Caritat, G. Tack, D. Laing, M.H. Zia, Chemosphere 74 (2009) 1279.

[21] Ch. Liua, R. Baib, Q.S. Lya, Water Res. 42 (2008) 1511.

[22] X. Zhang, Sh. Lin, Z. Chen, M. Megharaj, R. Naidu, Water Res. 45 (2011) 3481.

[23] D. Peixin, W. Huaxian, S. Hongjuan, Non-Metallic Mines 35 (2012) 57.

[24] P. Srivastava, B. Singh, M. Angove, J. Colloid Interface Sci. 290 (2005) 28.

[25] E. Erdem, N. Karapinar, R. Donat, J. Colloid Interface Sci. 280 (2004) 309.

[26] T.S. Jamil, H.S. Ibrahim, I.H. Abd El-Maksoud, S.T. El-Wakeel, Desalination 258 (2010) 34.

[27] Y. Tan, M. Chen, Y. Hao, Chem. Eng. J. 191 (2012) 104.

[28] M. Machida, B. Fotoohi, Y. Amamo, L. Mercier, Appl. Surf. Sci. 258 (2012) 7389.

[29] S.F. Lo, S.Y. Wang, M.J. Tsai, L.D. Lin, Chem. Eng. Res. Des. 90 (2012) 1397.

[30] D.T.C. Nguyen, H.T.N. Le, T.S. Do, V.T. Pham, D.L. Tran, V.T.T. Ho, T.V. Tran, D.C. Nguyen, T.D. Nguyen, L.G. Bach, H.K.P. Ha, V.T. Doan, J. Chem. https://doi.org/10.1155/2019/5602957.

[31] M. Ghanbarian, S. Zeinali, A. Mostafavi, Sens. Actuators B 267 (2018) 381.

[32] K. Sanderson,.Nature 448 (2007) 746.

[33] T.V. Tran, D.T.C. Nguyen, H.T.N. Le, T.T.K. Tu, N.D. Le, K.T. Lim, L.G. Bach, T.D. Nguyen, J. Environ. Chem. Eng. 7 (2019) 102881.

[34] G. Antek, W.F. Adam, J. Matzger, O.M. Yaghi, J.

Am. Chem. Soc. 128 (2006) 3494.
[35] Y.K. Seo, G. Hundal, I.T. Jang, Y.K. Hwang, C.H. Jun, J.S. Chang, Microporous Mesoporous Mater. 119 (2009) 331.
[36] J.S. Choi, W.J. Son, J. Kim, W.S. Ahn, Microporous Mesoporous Mater. 116 (2008) 727.
[37] W.J. Son, J. Kim, J. Kim, W.S. Ahn, Chem. Commun. 47 (2008) 6336.
[38] Z.Q. Li, L.G. Qiu, T. Xu, Y. Wu, W. Wang, Z.Y. Wu, X. Jiang, Mater. Lett. 63 (2009) 78.
[39] R. Ameloot, L. Stappers, J. Fransaer, L. Alaerts, B.F. Sels, D.E. DeVos, Chem. Mater. 21 (2009) 2580.
[40] S. Palaniandy, K.A.M. Azizli, Int. J. Miner. Process 92 (2009) 22.
[41] P. Amo-Ochoa, G. Givaja, P.J.S. Miguel, O. Castillo, F. Zamora, Inorg. Chem. Commun. 10 (2007) 921.
[42] W. Liu, L. Ye, X. Liu, L. Yuan, X. Lu, J. Jiang, Inorg. Chem. Commun. 11 (2008) 1250.
[43] Y. Yoo, Z. Lai, H.K. Jeong, Microporous Mesoporous Mater. 123 (2009) 100.
[44] C. Leonelli, T.J. Mason, Chem. Eng. Process. Process Intensif. 49 (2010) 885.
[45] A. De La Hoz, Á. Díaz-Ortiz, A. Moreno, Chem. Soc. Rev. 34 (2005) 164.
[46] G. Férey, Chem. Soc. Rev. 37 (2008) 191.
[47] C. Serre, F. Millange, C. Thouvenot, M. Nogues, G. Marsolier, D. Louer, G. Férey, J. Am. Chem. Soc. 124 (2002) 13519.
[48] F. Millange, N. Guillou, R.I. Walton, J.M. Greneche, I. Margiolaki, G. Férey, Chem. Commun. (2008) 4732.
[49] J.P.S. Mowat, S.R. Miller, A.M.Z. Slawin, V.R. Seymour, S.E. Ashbrook, P.A. Wright, Microporous Mesoporous Mater. 142 (2011) 322.
[50] T. Loiseau, C. Serre, C. Huguenard, G. Fink, F. Taulelle, M. Henry, T. Bataille, G. Ferey, Chem. Eur. J. 10 (2004) 1373.
[51] C. Volkringer, T. Loiseau, N. Guillou, G. Férey, E. Elkaim, A. Vimont, Dalton Trans. (2009) 2241.
[52] S. Heydari, M. Hosseinpour Zaryabi, H. Ghiassi, Anal. Bioanal. Chem. Res. 6 (2019) 271.
[53] T. Loiseau, C. Serre, C. Huguenard, G. Fink, F. Taulelle, M. Henry, T. Bataille, G. Ferey, Chem. Eur. J. 10 (2004) 1373.
[54] T.R. Whitfield, X. Wang, L. Liu, A.J. Jacobson, Solid State Sci. 7 (2005) 1096.
[55] L. Peng, J. Zhang, J. Li, B. Han, Z. Xue, G. Yang, Chem. Commun. 48 (2012) 8688.
[56] P. Horcajada, C. Serre, G. Maurin, N.A. Ramsahye, F. Balas, M. Vallet-Regi, M. Sebban, F. Taulelle, G. Ferey, J. Am.Chem. Soc. 130 (2008) 6774.
[57] T. Devic, P. Horcajada, C. Serre, F. Salles, G. Maurin, B. Moulin, D. Heurtaux, G. Clet, A. Vimont, J.M. Greneche, B. Le Ouay, F. Moreau, E. Magnier, Y. Filinchuk, J. Marrot, J.C. Lavalley, M. Daturi, G. Ferey, J. Am. Chem. Soc. 132 (2010) 1127.
[58] A. Banerjee, R. Gokhale, S. Bhatnagar, J. Jog, M. Bhardwaj, B. Lefez, B. Hannoyer, S. Ogale, J. Mater. Chem. 22 (2012) 19694.
[59] R. Fazaeli, H. Aliyanb, M. Moghadam, M. Masoudinia, J. Mol. Catal. A: Chem. 374 (2013) 46.
[60] J. Gordon, H. Kazemian, S. Rohani, Mater. Sci. Eng. C 47 (2015) 172.
[61] T.A. Vu, G.H. Le, C.D. Dao, L.Q. Dang, K.T. Nguyen, Q.K. Nguyen, P.T. Dang, H.T.K. Tran, Q.T. Duong, T.V. Nguyen, G.D. Lee, RSC Adv. 5 (2015) 5261.
[62] A. Nezamzadeh-Ejhieh, M. Kabiri-Samani, J. Hazard. Mater. 260 (2013) 339.
[63] M.A. Shavandi, Z. Haddadian, M.H.S. Ismail, N. Abdullah, Z.Z. Abidin, J. Taiwan, Inst. Chem. Eng. 43 (2012) 750.
[64] Y. Ren, J. Ma, Chem. Eng. J. 175 (2011) 1.
[65] Z.C. Li, H.T. Fan, Y. Zhang, M.X. Chen, Z.Y. Yu, X.Q. Cao, T. Sun, Chem. Eng. J. 171 (2011) 703.
[66] I.H. Gubbuk, J. Hazard. Mater. 186 (2011) 416.
[67] I.A Sengil, M. Ozacar, H. Turkmenler, J. Hazard. Mater. 162 (2009) 1046.
[68] N.M. Mahmoodi, B. Hayati, M. Arami, J. Chem. Eng. Data 55 (2010) 4638.
[69] J. Anwar, U. Shafique, W. Zaman, M. Salman, A. Dar, Sh. Anwar, Bioresour Technol. 101 (2010) 1752.
[70] J. Li, X. Wang, B. Yuan, M. Fu, H. Cui, Appl. Surf. Sci. 320 (2014) 112.
[71] M. Li, Z. Zhang, R. Li, J. Wang, A. Ali, Int. J. Biol. Macromol. 86 (2016) 876.

[72] K. Chen, J. He, Y. Li, X. Cai, K. Zhang, T. Liu, Y. Hu, D. Lin, L. Kong, J. Liu, J. Colloid Interface Sci. 494 (2017) 307.

[73] B. Guo, F. Deng, Y. Zhao, X. Luo, S. Luo, C. Au, Appl. Surf. Sci. 292 (2014) 438.